Proceedings of the ASME 2026 International Design Engineering Technical Conferences & Computers and Information in Engineering Conference
ASME IDETC/CIE2026
August 23 – 26, 2026, Houston, TX

ASME-IDETC2026-194256

DESIGN ARCHITECTURE OF A CYBER-PHYSICAL SMALL MODULAR REACTOR EMULATOR FOR REAL-TIME CONTROL AND GRID INTERACTION

Korebami O. Adebajo[1], Nathaniel Cooper[1], Ali Mahboub Rad[2,3], Matthew Whetham [1]Nolan Shute[1], Andrew Huebner[1], Austin R.J. Downey[1,4,*], Jie Zhang[2,3], Jamil Khan[1], Travis Knight[1],

[1]Department of Mechanical Engineering, University of South Carolina, Columbia, USA
[2]Department of Mechanical Engineering, University of Texas at Dallas, Texas, USA
[3]Department of Electrical and Computer Engineering, University of Texas at Dallas, Texas, USA
[4]Department of Civil and Environmental Engineering, University of South Carolina, Columbia, USA

ABSTRACT

Small Modular Reactors (SMRs) offer lower capital investment, enhanced siting flexibility, and modular construction advantages for distributed power generation. They are well-suited for manufacturing, remote sites, and military applications. Validating SMR control strategies and grid integration requires platforms that combine physical thermal dynamics with digital prediction models. Most existing models are purely computational simulations. These simulations may not capture hardware constraints, sensor noise, or actuator dynamics. This work presents the design architecture of a cyber-physical SMR emulator composed of three interacting subsystems: a physical primary thermal loop testbed and two cyber subsystems representing reactor dynamics and the secondary power conversion cycle. The reactor dynamics subsystem employs point-kinetics equations to compute neutron flux and thermal power generation, which determines the heat input applied to the physical primary loop. The primary loop testbed uses an electrically heated nichrome fuel rod emulator to generate the desired reactor thermal output, circulating water through a heat exchanger while monitoring pressure and temperature with industrial sensors. The secondary loop is a cyber subsystem that uses physics-based modeling to predict steam generation, turbine response, and electrical power output based on measured primary loop thermal conditions. System scaling employs time constant matching at the interface of the cyber and physical subsystems to preserve dynamic response characteristics. This platform provides a foundation for future validation of advanced control strategies for digitized control systems and grid integration protocols for next-generation SMR deployments.

Keywords: Small modular reactor (SMR), cyber-physical systems, hardware-in-the-loop testing, thermal-hydraulic control, digital twin

*Corresponding author: austindowney@sc.edu

1. INTRODUCTION

Small Modular Reactors represent a transformative approach to meeting energy demands through their diverse energy ranges and modular structures, particularly in remote areas [1]. This is especially true in the era of rising electricity consumption driven by data centers, AI infrastructure, and electrification initiatives [2]. SMRs extend these benefits through portability and scalability, enabling deployment in remote industrial sites, military installations, manufacturing facilities, and distributed grid applications where traditional large-scale reactors prove impractical [3]. The thermal-to-electrical conversion process in SMRs requires precise coordination between primary heat generation and secondary power cycles, especially as these reactors are increasingly expected to provide load-following capability in microgrids and low-inertia power systems, making robust control system validation important for operational stability [4, 5].

Cyber-physical validation platforms are necessary for testing advanced SMR control strategies under realistic operating conditions that capture both thermal dynamics and real-time electric grid interactions. Traditional approaches rely on purely computational simulations that cannot replicate hardware constraints such as sensor noise, actuator delays, communication latency, and component degradation [6]. A cyber-physical platform enables parallel operation of physical thermal systems alongside predictive digital models, allowing operators to assess system behavior under load-following scenarios, grid disturbances, and fault conditions before deployment. This coupled approach informs design decisions for pressure management systems, temperature control loops, and grid synchronization protocols with higher fidelity than simulation-only methods.

Other related research in this area has primarily focused on safeguarding SMRs from cybersecurity threats to build regulatory and public confidence in their widespread deployment [7]. The increased interest in advanced reactors has also ignited research into deep-learning architectures, such as wavy-attention networks, designed to detect real-time cyber-attacks within highly digitized SMR digital control systems [8]. Parallel to cybersecurity efforts, recent work has begun exploring control-oriented digital twins and real-time hardware-in-the-loop (HIL) frameworks to simulate SMR nuclear dynamics for microgrid stability and nuclear-renewable hybrid energy dispatch [9, 10]. These research assessed HIL integration through setup specified for the microgrid systems and not the main fluid system which is accounted for here.

Integrated hardware-software architectures that combine scaled thermal testbeds with real-time digital twins remain scarce in SMR research. Integrated hardware-software architectures that combine scaled thermal testbeds with real-time digital twins remain scarce in SMR research. However, large-scale SMR deployments would benefit from digital twins for real-time control and advanced predictive diagnostics during critical, un-monitored transient states. The predictive capabilities could allow the control system to either avoid fault conditions or guide operators in emergency situations. The platform combines a scaled physical primary loop with real-time digital secondary loop simulation, creating a HIL environment where thermal measurements drive electrical predictions. The primary loop uses electric heaters to emulate reactor thermal output, with a multi-physics model (Simulink/Simscape) running in parallel to validate thermal predictions. Nuclear behavior is represented through point kinetics neutronics models that calculate reactivity balance and thermal power output, feeding temperature changes to both the physical testbed heater and the primary loop digital model [11]. The secondary thermal loop, including steam generation, turbine dynamics, and electrical conversion, operates entirely in simulation, accepting measured primary loop conditions as boundary inputs. The cyber subsystems are implemented as physics-based models (Simulink/Simscape) designed for future deployment on real-time control hardware (Speedgoat) to enable HIL experimentation.

Time constant matching at the interface of the cyber and physical subsystems ensures dynamic similarity between the scaled testbed and full-scale SMR systems by preserving control response characteristics across different physical scales. We employ dimensionless time ratios analogous to the Fourier number, comparing heat diffusion rates to characteristic process timescales to maintain proportional thermal dynamics. System time constants are normalized to characteristic process times, allowing control algorithms to scale appropriately between the testbed and commercial reactor systems. Time-based responses are derived from fluid temperature rise at the two thermal interfaces which govern the interaction between the three subsystems: the rod-to-coolant interface within the heated test section and the steam generator interface between the primary and secondary loops. The rod-to-coolant interface couples the reactor dynamics subsystem with the physical primary loop by translating neutronically predicted heat generation into thermal energy transferred to the circulating coolant. The steam generator interface couples the physical primary loop to the secondary power cycle model through heat exchange that drives steam generation and turbine dynamics. Establishing the fundamental timescale for each subsystem and enabling coordinated simulation timing across nuclear, primary

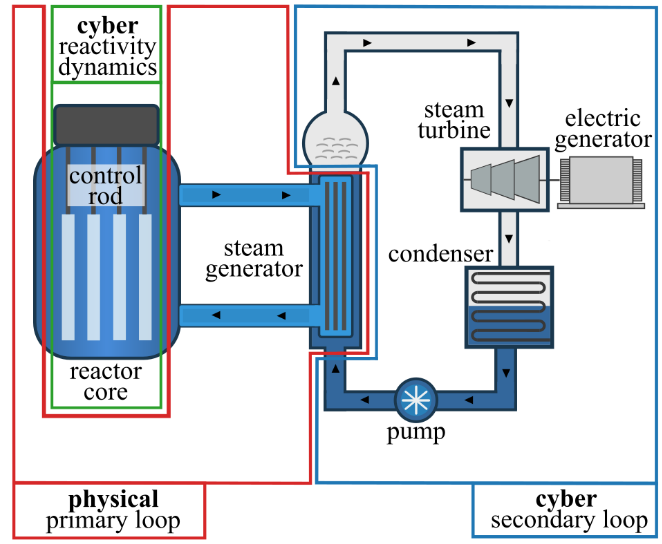

FIGURE 1: Subsystem architecture of the cyber-physical SMR emulator showing the interaction between the reactor dynamics (cyber), primary thermal loop testbed (physical), and secondary power cycle model (cyber).

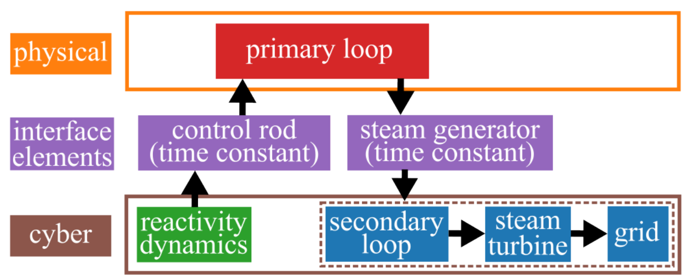

FIGURE 2: Domain-level abstraction of the cyber-physical SMR architecture illustrating the separation of cyber models and physical hardware and the interfaces that couple them.

thermal, and secondary electrical components.

This design architecture presents a cyber-physical SMR emulator that integrates scaled thermal hardware with real-time digital prediction models for comprehensive control validation. The platform provides a foundation for testing advanced control strategies, evaluating grid integration protocols, and assessing cybersecurity resilience in SMR systems before full-scale deployment. By combining measured thermal dynamics with predictive electrical models, the emulator enables experimental investigation of load-following performance, transient response characteristics, and multi-physics coupling effects that purely digital simulations cannot capture. The contributions of this work are threefold: (1) definition of subsystem interfaces linking the reactor dynamics, primary thermal loop, and secondary power-cycle models; (2) a time-constant-based scaling methodology preserving dynamic similarity between the testbed and full-scale SMR systems; and (3) development of a physical thermal-hydraulic testbed for hardware-in-the-loop control validation.

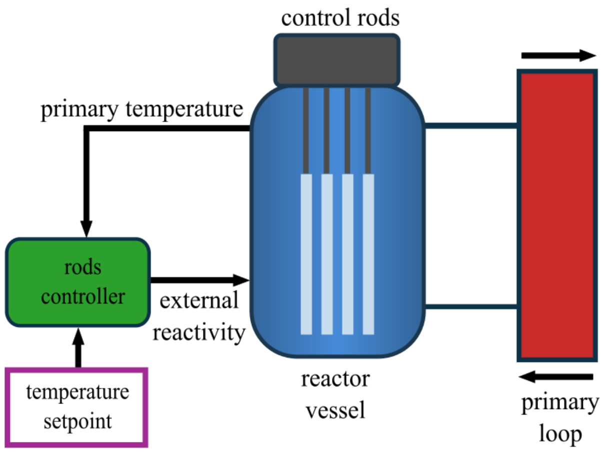

FIGURE 3: Reactor dynamics cyber subsystem computing neutron population dynamics and thermal power using point-kinetics equations.

FIGURE 4: Physical primary loop thermal-hydraulic testbed used to emulate reactor heat generation and coolant circulation with instrumented sensors.

2. METHODOLOGY

The cyber-physical SMR emulator integrates three coupled subsystems (one physical and two cyber) to enable real-time validation of reactor thermal and electrical dynamics. The first cyber subsystem is a nuclear reactivity model that computes heat generation from neutron kinetics equations and determines the thermal input applied to both the physical heater and the digital primary loop (discussed in Section 2.1). The physical primary thermal loop subsystem replicates the primary thermal loop of a SMR, providing measured temperature and pressure data that serve as operating conditions for the digital models (discussed in Section 2.2 The second cyber subsystem is a combined thermal and power model that simulates the primary and secondary loop behavior, including heat transfer, steam generation, turbine dynamics, and electrical output (discussed in Section 2.3).

2.1. Reactor Dynamics (Cyber Subsystem)

Figure 3 reports the organizational structure of the reactor dynamics sub system. The nuclear reactivity model predicts thermal power generation in the reactor core through point kinetics equations that govern neutron population dynamics and delayed neutron precursor concentrations. These equations couple reactor physics to thermal-hydraulic behavior by relating neutron flux to heat generation, which then determines the rod surface temperature boundary condition for both the physical testbed heater and the digital primary loop model.

The point kinetics equations consist of two coupled differential equations describing the rate of change of average neutron flux and delayed neutron precursor concentration

$$\frac{d\phi}{dt} = \left(\frac{\rho - \beta}{\Lambda}\right)\phi + \lambda C, \tag{1}$$

$$\frac{dC}{dt} = \frac{\beta}{\Lambda}\phi - \lambda C, \tag{2}$$

where $\phi(t)$ is the average neutron flux (population), $C(t)$ is the concentration of delayed neutron precursors, $\rho(t)$ is the reactivity introduced by changes in reactor conditions (control rod position, fuel burnup), β is the delayed neutron fraction, Λ is the prompt neutron lifetime, and λ is the decay constant for delayed neutron precursors.

Reactivity $\rho(t)$ accounts for control rod actuation and temperature feedback effects through fuel and coolant temperature deviations

$$\rho = \rho_{\text{ext}} + \alpha_{\text{f}}(\Delta T_{\text{f}}) + \alpha_{\text{c}}(\Delta T_{\text{c}}), \tag{3}$$

where ρ_{ext} is the reactivity due to control rod operation, α_{f} is the fuel temperature coefficient of reactivity, α_{c} is the coolant temperature coefficient of reactivity, $\Delta T_{\text{f}}(t)$ represents fuel temperature deviations from initial steady state, and $\Delta T_{\text{c}}(t)$ represents coolant temperature deviations from initial steady state. The temperature coefficients provide negative feedback that stabilizes reactor power output, as increases in fuel or coolant temperature reduce reactivity and slow the chain reaction.

The neutron flux solution from Eq. 1 is converted to thermal power output, which sets the heater power command for the physical testbed and the heat flow input for the digital primary loop model. Table 1 summarizes the neutronics parameters used in the point kinetics model.

TABLE 1: Reactor dynamics model parameters.

parameter	value
β (delayed neutron fraction)	0.007
Λ (prompt neutron lifetime)	$2{\times}10^{-5}$ s
λ (decay constant)	0.1 (1/s)
α_{f} (fuel temp. coefficient)	$-2.16{\times}10^{-5}$ (1/°C)
α_{c} (coolant temp. coefficient)	$-1.8{\times}10^{-4}$ (1/°C)

2.2. Primary Thermal Loop (Physical Subsystem)

The physical primary loop shown in Figure 4, provides a scaled representation of an SMR primary thermal circuit, enabling hardware-in-the-loop validation of the digital models described in subsequent sections. The testbed circulates water through a closed loop consisting of four main components: an electrically heated test section that emulates reactor core thermal output, a shell-and-tube heat exchanger that transfers thermal energy to a secondary cooling circuit, a centrifugal circulation pump, and instrumented piping with a controllable bypass path. The heated test section uses a nichrome resistance heating element powered by a 10 kW DC supply, with thermal output controlled to match temperatures predicted by the nuclear reactivity model. City water flows through the heat exchanger shell side at up to 1.8 m^3/hr, providing cooling similar to a secondary loop steam generator. The bypass valve, positioned upstream of the heat exchanger, enables flow control by diverting a fraction of the heated fluid around the heat exchanger and directly back to the pump inlet, allowing the testbed to emulate varying thermal loads without modifying heater power. A public repository with models and data for the system is provided by the authors [12].

Instrumentation distributed throughout the loop captures pressure, temperature, and flow rate at different key locations for model validation and closed-loop control. Three pressure transducers monitor inlet, mid-loop, and outlet pressures to detect pump performance and pressure drop characteristics. Seven Type K thermocouples measure fluid temperatures at the heater inlet and outlet, heat exchanger inlet and outlet, pump inlet, and bypass junction points. A turbine flow meter positioned downstream of the pump records volumetric flow rate. Major components and sensor placements can be observed in figure 4 highlighting the setup. All sensor signals are acquired at 10 Hz using a National Instruments CompactDAQ chassis mounted on the testbed frame, with data logged for post-experiment analysis. The table below summarizes the key component specifications and nominal operating conditions [13].

TABLE 2: Primary thermal loop specifications.

parameter	value
heater power supply	10 kW
pump max flow rate	15 m^3/h at 10 m head
pump max temperature	180 °C
heat exchanger capacity	1.8 m^3/h
pressure transducers	3 (0–5 bar)
thermocouples	7 (Type K)
flow meter range	0–20 m^3/h
nominal flow rate	14.5 m^3/h
reactor inlet temp	103.1 °C
reactor outlet temp	103.5 °C
temperature rise	0.4 °C
thermal power added	7 kW
nichrome rod diameter	9.5 mm
nichrome rod pitch	12.6 mm

Control of the testbed is achieved through two independent actuators power modulation for the electrically heated fuel rod emulator (commanded by the nuclear reactivity model) and bypass valve position (commanded by the primary loop level or flow controller). The bypass valve allows flow distribution between the heat exchanger and bypass paths without requiring variable-speed pump control, simplifying the mechanical system while maintaining the ability to emulate load-following scenarios. At the fully closed bypass position, all flow passes through the heat exchanger for maximum cooling; at the fully open position, a portion of the flow recirculates directly to the pump, reducing effective heat rejection and allowing fluid temperature to rise. This configuration mimics the thermal response of an SMR primary loop under varying secondary-side steam demand.

In addition to the physical testbed, a multi-physics virtual representation of the primary loop is developed to replicate the thermal–hydraulic behavior of the system and provide a basis for comparison with measured data. This pairing of the physical system with its virtual representation constitutes a digital twin, in which the virtual representation mirrors the behavior of its physical counterpart [14].

The primary loop virtual representation replicates the thermal–hydraulic behavior of the physical loop. Implemented using Simulink/Simscape, this multi-physics representation enables parallel prediction and validation of temperature, pressure, and flow dynamics within the loop. The virtual representation employs thermal fluid domain blocks from the Simscape Thermal Fluids library to represent each major physical component, including the circulation pump, heated fuel rod channel, main circulation piping, bypass path, and heat exchanger. The virtual representation is designed for future deployment on a real-time target machine (Speedgoat), where it receives heater power commands from the reactor dynamics subsystem and outputs predicted thermal conditions to the secondary loop model.

Fluid flow in the virtual representation follows the same path as the physical system: the pump drives water through the fuel rod channel where thermal power (commanded by the reactor dynamics model) is applied via a prescribed heat flow block, then through the main pipe to a T-junction where flow splits between the bypass path and heat exchanger branch, and finally returns to the pump inlet to close the loop. The heat exchanger block represents the steam generator interface between primary and secondary circuits, modeled as a controlled heat sink with specified cooling water inlet temperature and variable flow rate. The secondary-side cooling flow is implemented using a flow rate source connected to a constant-temperature reservoir, allowing simulation of varying heat rejection rates that correspond to different secondary-side steam demands. Pipe segments throughout the virtual representation include thermal mass and convective heat loss to ambient conditions (detailed at 23°C) to capture transient heating effects and steady-state losses observed in the physical testbed.

Sensor blocks in the virtual representation are positioned at identical locations to the physical testbed instrumentation: pressure sensors at pump inlet, mid-loop, and heat exchanger outlet; temperature sensors at the reactor inlet/outlet, heat exchanger inlet/outlet, and bypass junction; and a flow meter downstream of the pump. These virtual sensors provide direct comparison points for virtual representation validation against experimental data.

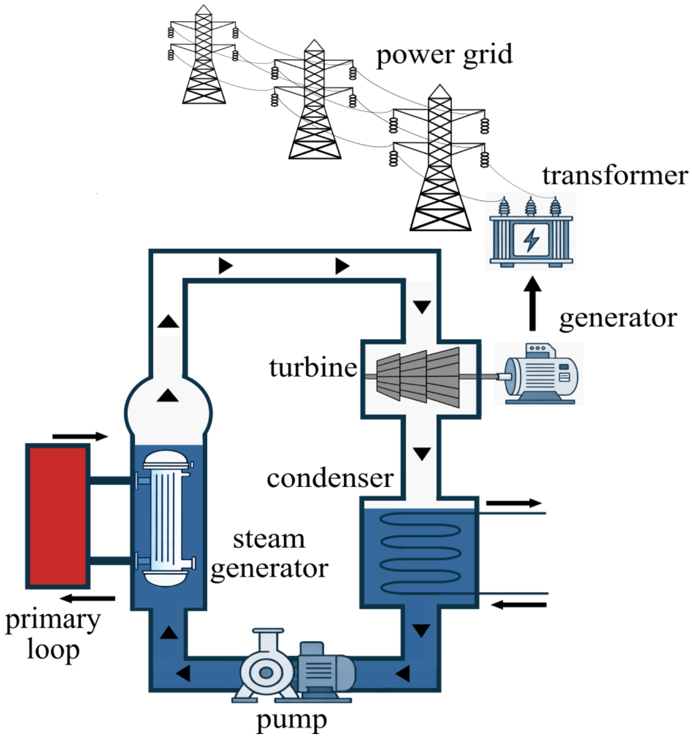

FIGURE 5: Subsystem of the cyber secondary loop that converts primary loop thermal energy into electrical output.

2.3. Secondary Power Cycle (Cyber Subsystem)

The secondary loop digital model is shown in Figure 5 and simulates the Rankine thermodynamic cycle that converts primary loop thermal energy into electrical power through steam generation, turbine expansion, and condensation. Unlike the primary loop, which has both physical and digital representations, the secondary loop exists only as a multi-physics model (Simulink/Simscape) due to the higher pressures, temperatures, and mechanical complexity required for accurate turbine operation. The model uses two-phase fluid domain blocks in Simscape to capture boiling, super-heating, expansion, and condensation processes that occur throughout the steam cycle. Thermal energy from the primary loop heat exchanger outlet is transferred to the secondary side through the steam generator (boiler) block, where liquid water is heated to saturated or super-heated steam at elevated pressure. The working fluid begins at hot startup conditions with an initial pressure of 1.4 MPa and receives 4.5 MW of thermal input from the steam generator, representative of steady-state operation following reactor startup procedures. Steam exits the generator and flows through insulated piping to the turbine block, which models isentropic expansion with mechanical efficiency losses to convert thermal energy into rotational shaft work. The turbine is coupled to a mechanical rotational domain with a target capacity of 1 MW under nominal conditions. Current model efficiency stands at 20% (turbine electrical output divided by thermal input).

After expansion through the turbine, low-pressure steam enters a condenser block where it is cooled by a heat exchanger through a separate cooling water system. The condenser rejects waste heat to return the working fluid to a saturated liquid state for turbine operation. A controlled mass flow rate source positioned between the condenser outlet and steam generator inlet acts as the feedwater pump, maintaining circulation and allowing control system testing. The flow rate is modulated based on steam generator liquid level feedback to prevent dryout or overfilling. Control of the secondary loop is achieved through two primary modes: the feedwater mass flow rate and the steam generator heat input. The bypass valve mentioned in the primary loop description indirectly affects secondary loop performance by modulating heat exchanger effectiveness, creating a coupled thermal response between the two systems. Figure 5 shows the major components modeled, including the steam generator, turbine, condenser, feedwater pump, and any sensors used. Table 3 summarizes the key operating parameters and component ratings.

TABLE 3: Secondary power cycle specifications.

parameter	value
initial pressure	1.4 MPa
steam generator heat input	4.5 MW
target turbine output	1 MW
cycle efficiency	20%
working fluid	water (2-phase)
condenser cooling	heat sink (ambient)
feedwater control	mass flow rate source

TABLE 4: Time-based scaling factor, time constants for the 2 interface elements.

	heated fuel rod		heat exchanger
	part 1	part 2	
τ (sec | min)	0.7 | 0.02	50.4 | 0.84	179 | 2.98

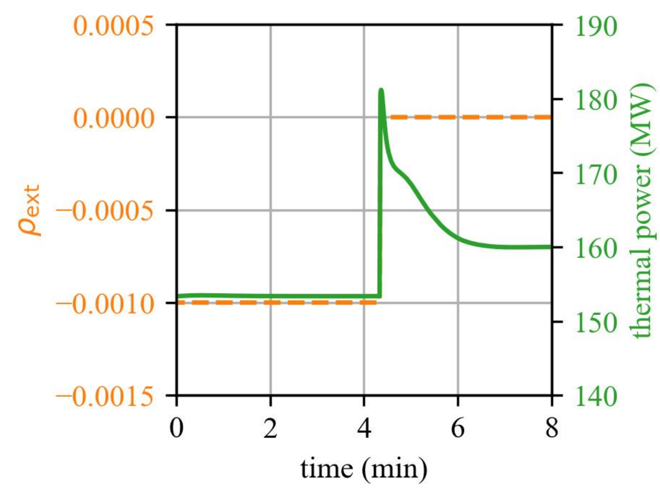

FIGURE 6: Transient thermal response at the rod–coolant interface following a step change in control rod position predicted by the reactor dynamics subsystem.

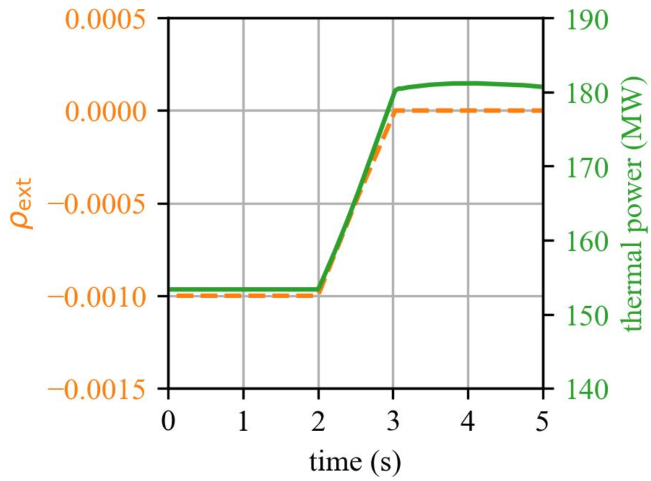

FIGURE 7: Transient thermal response of the first part at the rod–coolant interface following a step change in control rod position predicted by the reactor dynamics subsystem.

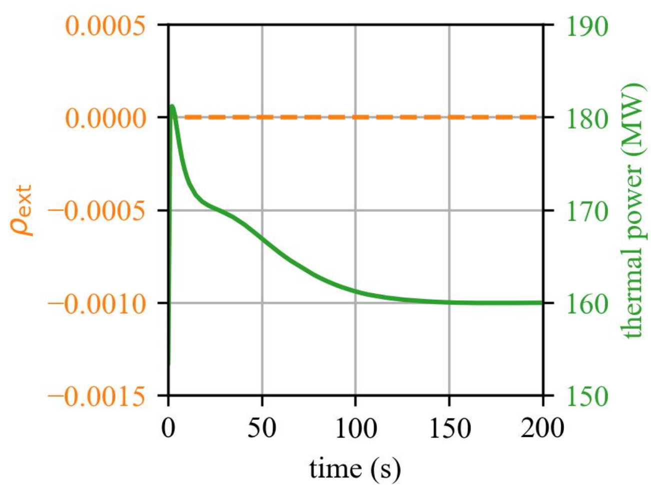

FIGURE 8: Transient thermal response of the second part at the rod–coolant interface following a step change in control rod position predicted by the reactor dynamics subsystem.

3. SCALING METHODOLOGY AND INTEGRATION ARCHITECTURE

Scaling between the laboratory testbed and full-scale SMR systems is achieved through time constant matching rather than geometric scaling. The characteristic time constant for each subsystem's intersection represents its thermal response speed and determines the required control system bandwidth. For the primary loop, the time constant is defined as the thermal response time of the heat transfer components under nominal operating conditions. Two primary time constants govern the testbed dynamics: the electrically heated fuel rod emulator thermal response (τ_{rod} = 0.84 min) and the heat exchanger thermal response (τ_{HX} = 2.98 min), as shown in Table 4. These time scales represent the speed at which each component responds to changes in thermal input or flow conditions.

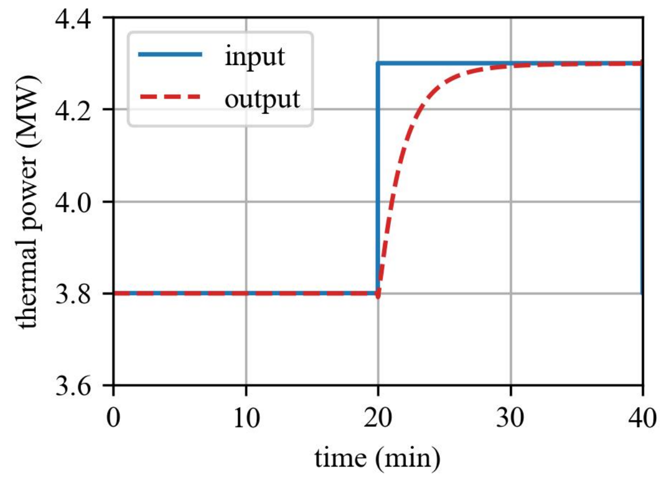

FIGURE 9: Transient outlet energy response at the steam generator interface following a step change in thermal input from the primary loop.

The heated fuel rod emulator time constant of 0.84 min captures the thermal inertia of the electrically heated test section, governing how quickly the rod surface temperature responds to power input changes. This is shown in figures 7 and 8 fixating of the initial rapid ascent then in the later figure the decline to steady state. The heat exchanger time constant of 2.98 min reflects the larger thermal mass and fluid inventory in the shell-and-tube heat exchanger, resulting in a slower transient response. These values were derived from results shown in figures 6 and 9, respectively. Figure 9 shows the power introduced to the secondary loop compared to the change observed in the fluid over time. Similarly, the secondary loop introduces time constants associated with steam generator pressure dynamics and turbine-condenser mass transfer processes, while the nuclear reactivity model contributes time scales related to delayed neutron precursor decay (on the order of seconds to tens of seconds based on the decay constant $\lambda = 0.1$ s^{-1} from Table 1).

Preserving the ratios between these time constants ensures that coupled thermal-hydraulic-neutronics behavior scales appropriately across different physical sizes. Control system performance depends on the dimensionless ratio of control sample time to process time constant. If testbed time constants are faster than full-scale SMR systems by a scaling factor α, then control algorithms must operate with proportionally faster update rates to maintain equivalent closed-loop stability margins and transient response characteristics. This dimensionless scaling approach allows control strategies validated on the testbed to transfer directly to commercial reactor systems with predictable performance.

Future refinement of the scaling methodology will incorporate additional control-specific parameters, such as steady-state and transient temperature differences across heat transfer components during load-following scenarios. These supplementary factors can improve prediction accuracy for coupled system behavior where thermal lag and transport delays interact with feedback control loops.

4. CONCLUSION

This work presents the design architecture for a cyber-physical SMR emulator that combines scaled physical hardware with digital prediction models to enable control system validation. The platform integrates three coupled subsystems: a nuclear reactivity model computing thermal power from neutron kinetics, a physical primary loop testbed providing measured thermal-hydraulic data, and digital models of the primary and secondary loops predicting system behavior. Scaling between the laboratory testbed and full-scale SMR systems is achieved through time constant matching, where characteristic thermal response times for each subsystem are normalized to preserve dynamic similarity and control bandwidth relationships.

The primary scaling approach relies on matching dimensionless ratios of process time constants across the nuclear, primary thermal, and secondary electrical subsystems. For the primary loop, the time constant is derived from the temperature rise across the heated section under nominal power input, providing a characteristic timescale that can be compared to full-scale reactor coolant dynamics. The design provides a foundation for future experimental validation of advanced control algorithms, cyber-attack resilience testing for digitized control rooms, and grid integration protocol development. Future work will incorporate additional scaling factors based on control-specific parameters, such as the temperature difference across heat exchanger components during transient operation, to improve accuracy in coupled thermal-hydraulic response prediction.

ACKNOWLEDGMENTS

This material is based upon work supported by the AQSEL project funded by The South Carolina Quantum Association/State of South Carolina Additional funding for this work comes from the National Science Foundation (NSF) through grant number CPS - 2237696. Any opinions, findings, conclusions, or recommendations expressed in this material are those of the authors and do not necessarily reflect the views of The South Carolina Quantum Association or the National Science Foundation.

REFERENCES

[1] DOE, US. "Benefits of Small Modular Reactors (SMRs)." URL https://www.energy.gov/ne/benefits-small-modular-reactors-smrs.

[2] IEA. *Electricity 2026*. International Energy Agency, Paris (2026). URL https://www.iea.org/reports/electricity-2026. Licence: CC BY 4.0.

[3] Wang, Y., Chen, W., Zhang, L., Zhao, X., Gao, Y. and Dinavahi, V. "Small Modular Reactors: An Overview of Modeling, Control, Simulation, and Applications." *IEEE Access* Vol. 12 (2024): pp. 39628–39650. DOI 10.1109/ACCESS.2024.3351220.

[4] Park, Kibeom, Park, Tongkyu, Zee, Sung Kyun and Koo, Bon Seung. "Control rod driven long-term load-follow operation in small modular reactor." *Annals of Nuclear Energy* Vol. 182 (2023): p. 109620. DOI 10.1016/j.anucene.2022.109620. URL https://www.sciencedirect.com/science/article/pii/S0306454922006508.

[5] Michaelson, D. and Jiang, J. "Review of integration of small modular reactors in renewable energy microgrids." *Renewable and Sustainable Energy Reviews* Vol. 152 (2021): p. 111638. DOI 10.1016/j.rser.2021.111638. URL https://www.sciencedirect.com/science/article/pii/S1364032121009138.

[6] Diaz-Pescador, E., Bilodid, Y., Jobst, M. and Kliem, S. "NuScale-like SMR Model Development and Applied Safety Analyses with the Code Chain Serpent-DYN3D-ATHLET." *Nuclear Engineering and Design* Vol. 418 (2024): p. 112909. DOI 10.1016/j.nucengdes.2024.112909. URL https://www.sciencedirect.com/science/article/pii/S0029549324000116.

[7] Zamperini, Michael B. and Schwerha, Diana J. "Simulating Collaboration in Small Modular Nuclear Reactor Cybersecurity with Agent-Based Models." *Journal of Cybersecurity and Privacy* Vol. 5 No. 4 (2025). DOI 10.3390/jcp5040083. URL https://www.mdpi.com/2624-800X/5/4/83.

[8] Ayodeji, Abiodun, Di Buono, Antonio, Pierce, Iestyn and Ahmed, Hafiz. "Wavy-attention network for real-time cyber-attack detection in a small modular pressurized water reactor digital control system." *Nuclear Engineering and Design* Vol. 424 (2024): p. 113277. DOI https://doi.org/10.1016/j.nucengdes.2024.113277. URL https://www.sciencedirect.com/science/article/pii/S0029549324003777.

[9] Gabbar, Hossam A. and Esteves, Otavio Lopes Alves. "Real-Time Simulation of a Small Modular Reactor in-the-Loop within Nuclear-Renewable Hybrid Energy Systems." *Energies* Vol. 15 No. 18 (2022). DOI 10.3390/en15186588. URL https://www.mdpi.com/1996-1073/15/18/6588.

[10] Almukhametov, Akzhol, Lim, Doyeong, Hu, Rui and Liu, Yang. "Graph Neural ODE Digital Twins for Control-Oriented Reactor Thermal-Hydraulic Forecasting Under Partial Observability." (2026). URL 2604.07292, URL https://arxiv.org/abs/2604.07292.

[11] Duderstadt, J J and Hamilton, L J. *Nuclear reactor analysis*. John Wiley and Sons, Inc.,New York (1976). URL https://www.osti.gov/biblio/7355364.

[12] ARTS-Lab. "thermal loop." GitHub (2025). URL https://github.com/ARTS-Laboratory/thermal-loop.

[13] Carrilho, Leo Alves. "Experimental and Computational Study of Roughened Surface For PWR Rod Bundles." phdthesis, University of South Carolina. 2012. URL https://scholarcommons.sc.edu/etd/2223.

[14] National Academy of Engineering and National Academies of Sciences, Engineering, and Medicine. *Foundational Research Gaps and Future Directions for Digital Twins*. The National Academies Press, Washington, DC (2024). DOI 10.17226/26894. URL https://nap.nationalacademies.org/catalog/26894/foundational-research-gaps-and-future-directions-for-digital-twins.